EDGE ARTICLE

Check for updates

All publication charges for this article have been paid for by the Royal Society of Chemistry

Plasmon-powered chemistry with visible-light active copper nanoparticles†

Shreya Tyagi, [ID] Radha Krishna Kashyap, [ID] Ankit Dhankhar and Pramod P. Pillai [ID] *

In the quest for affordable materials for performing visible-light driven chemistry, we report here intriguing optical and photothermal properties of plasmonic copper nanoparticles (CuNPs). Precise tuning of reaction conditions and surface functionalization yield stable and monodisperse CuNPs, with a strong localized surface plasmon absorption at ∼580 nm. The molar extinction coefficient is estimated to be ∼7.7 × 10^7 M^{-1} cm^{-1} at 580 nm, which signifies their suitability for various light-harnessing studies. The characteristic wine-red colour and crystallography studies confirm the presence of mainly Cu(0) atoms in CuNPs, which showed excellent long-term colloidal and compositional stability under ambient conditions (at least 50 days). The as-synthesized oleylamine-capped CuNPs are ligand-exchanged with charged thiolate ligands of both polarities to form stable dispersions in water, with complete retention of their plasmonic properties and structural integrity (for ∼2 days and ∼6 h under inert and ambient conditions, respectively). Photothermal-conversion efficiency of CuNPs is estimated to be ∼80%, raising the surrounding temperature to ∼170 °C within ∼30 s of irradiation with a 1 W 532 nm diode laser, which is 'hot' enough to perform useful solar-vapor generation and high-temperature crystal-to-crystal phase transformation. Our work projects plasmonic CuNPs as an affordable and effective alternative to conventional metal NPs to harness light–matter interactions for future plasmon-powered chemistry.

Introduction

Non-radiative thermal deactivation process is one of the most spontaneous events occurring in the majority of solar absorbers, wherein the absorbed solar energy is eventually dissipated as heat to the local surroundings.[1–6] This heat dissipated from photoexcited materials can increase the temperature of the surrounding medium, in some cases, by hundreds of degrees Celsius.[7–9] Thus, the utilization of the heat dissipated in light-induced processes is essential to maximize the effective harnessing of solar energy. This has inspired researchers to develop efficient photothermal materials and use the dissipated heat for driving energy-intensive processes with light.[10–12] In this direction, metal nanomaterials have achieved a special feat[13–17] because of their unique localized surface plasmon properties.[1–6,18] Optical excitation induces a collective and coherent oscillation of a 'sea of electrons' in metal nanoparticles (NPs), which under the resonance conditions leads to exceptionally high absorption and concentration of the light

energy (the molar extinction cross-section of metal NPs is 4–6 orders higher than that of conventional dye molecules). This phenomenon is termed localized surface plasmon resonance (LSPR). Next, the light energy stored in a photoexcited plasmonic metal NP mainly decays *via* a series of non-radiative pathways, involving Landau damping, electron–electron, electron–phonon, and phonon–phonon scattering processes.[1–6] The overall non-radiative relaxation process is so fast that a plasmonic NP dissipates the absorbed light energy into heat within a few picoseconds of excitation, which is defined as plasmonic heat.[3] As the absorption cross-section is exceptionally high, the amount of plasmonic-heat dissipated by metal NPs is also huge (the surrounding temperature has been reported to rise up to ∼600 °C).[8] Now, the majority of these thermoplasmonic studies are conducted with metal NPs based on Au and Ag because of their excellent chemical stability and ease of chemical synthesis.[14–22] But the limited availability and cost of these metal precursors have triggered the search for more sustainable alternatives of plasmonic NPs[23] based on (i) affordable metals (Cu and Al),[24,25] (ii) metal carbides and nitrides (TiC and TiN),[26,27] and (iii) doped chalcogenides (CuS and In$_2$O$_3$).[28] Among them, plasmonic Cu(0)NPs have been theoretically predicted to have strong visible-light-driven thermoplasmonic properties like Au and Ag NPs.[29] Accordingly, appreciable efforts have been dedicated towards the development of CuNPs.[24] Most of these studies were mainly emphasized on the synthesis aspects, with limited focus on their optical and light-harvesting

Department of Chemistry and Centre for Energy Sciences, Indian Institute of Science Education and Research (IISER), Dr Homi Bhabha Road, Pashan, Pune – 411 008, India. E-mail: pramod.pillai@iiserpune.ac.in

properties.[30–33] For instance, the thermoplasmonic properties of CuNPs are less explored experimentally because of the challenges associated with their poor structural stability, size-uniformity, fast oxidation, and lack of colloidal stability in diverse solvents, including water.[24] As a result, there is only a limited set of data available on the optical and photothermal properties of CuNPs,[24,30–39] compared to their counterparts based on Au and Ag.[16–22] A few of the fundamental aspects that must be investigated immediately for CuNPs include molar extinction coefficient, ligand-exchange protocols, colloidal stability, photothermal conversion efficiency, and demonstration of plasmonic-heat driven high-temperature processes. Such a study is essential to strengthen the claim that CuNPs are an affordable thermoplasmonic material for future photothermal applications, and this forms the basis of the present work.

Herein, we report the synthesis, stability, surface functionalization, and plasmonic properties of CuNPs. The as-synthesized oleylamine-capped copper nanoparticles (OAm-CuNPs) in toluene showed excellent uniformity in size and shape, with an average core diameter of ~9.0 nm. A strong LSPR band was observed at ~580 nm, with the colloidal solution showing a wine-red color characteristic of Cu(0) NPs. The molar extinction coefficient (ε) was estimated to be ~7.7×10^7 M^{-1} cm^{-1} at 580 nm. This perhaps may be the first report of the molar extinction coefficient of well-dispersed colloidal CuNPs at the plasmon maximum. The as-synthesized OAm-CuNPs were found to be stable for at least 50 days under ambient conditions. Furthermore, the parent oleylamine ligands were replaced with both positively and negatively charged thiolate ligands to impart colloidal stability in the aqueous medium, without any compromise in their plasmonic properties and structural integrity (for ~2 days and ~6 h under inert and ambient conditions, respectively. Scheme 1). Interestingly, CuNPs could raise the surrounding temperature to ~170 °C, within ~30 s of illumination with a 532 nm continuous wave (CW) diode laser (light intensity was estimated to be 1 W cm^{-2}). Thermoplasmonic studies revealed that CuNPs showed an excellent photothermal efficiency of ~80%, which was sufficient to perform high-temperature reactions such as solar-vapor generation and crystal-to-crystal phase transformation. Thus, our work reports some of the key plasmonic properties of CuNPs, that signify the potency of CuNPs as alternate plasmonic heaters in harnessing light–matter interactions for future plasmon-powered processes. In this way, one can reduce the burden on conventional plasmonic materials based on precious metals for various light-harvesting applications.

## Results and discussion

Preparation of monodisperse CuNPs

Copper nanoparticles (CuNPs) were prepared by the high-temperature chemical reduction of copper(II) acetylacetonate (Cu(acac)$_2$), following a modified literature protocol.[40] Briefly, Cu(acac)$_2$ in oleylamine (OAm) was heated under an argon atmosphere to ~230 °C for 2 h (Fig. 1a). A series of color changes were observed within 2 h of heating: light blue → light
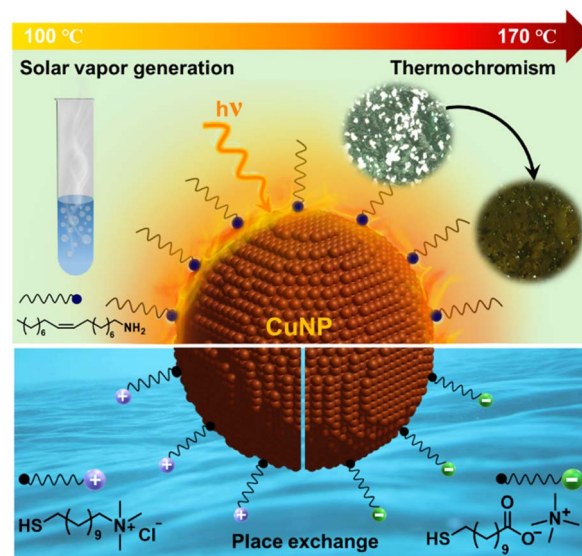
Scheme 1 A scheme highlighting the stable dispersions of plasmonic CuNPs in organic and aqueous media, along with their thermoplasmonic properties. Schematics of CuNPs functionalized with non-polar (OAm) and polar (charged thiolate) surface ligands, leading to stable dispersions in toluene and water, respectively. The plasmonic heat generated from illuminated CuNPs was 'hot' enough to perform high-temperature photothermal applications, such as solar-vapor generation and crystal-to-crystal phase transformation.

green → dark green → orange → black, and finally to deep red, indicating the successful formation of colloidal CuNPs (Fig. S1†). OAm acts as the reducing agent as well as the capping ligand in this synthesis. It must be noted that the synthesis of plasmonic CuNPs is not a trivial task, as it is highly susceptible to undergo oxidation. Thus, even though a modified literature procedure was adopted, additional precautions were taken in the present study to reduce the oxidation, such as (i) maintaining an inert atmosphere throughout the synthesis, (ii) purification with degassed solvents, (iii) minimal exposure of CuNPs during purification, and (iv) redispersion in a degassed solvent. These precautions turned out to be decisive in maintaining the long-term stability of the CuNPs in our study (*vide infra*). High-resolution transmission electron microscopy (HRTEM) analysis revealed the formation of highly monodisperse and spherical-shaped OAm-CuNPs, with an average diameter of 9.0 ± 1.1 nm (Fig. 1b and S2†). The interplanar spacing of 0.20, 0.18 and 0.13 nm corresponds to (111), (200) and (220) planes of Cu, respectively (see the inset of Fig. 1c). The appearance of a sharp LSPR band at ~580 nm further confirms the size and shape uniformity of OAm-capped CuNPs (Fig. 1d). The molar extinction coefficient (ε) of OAm-capped CuNPs was estimated to be ~7.7×10^7 M^{-1} cm^{-1} at 580 nm, with the help of ICP-MS, UV-vis absorption, and TEM studies (see the details in Section 4 of the ESI†). Such a high value of ε confirms the potential of CuNPs to exhibit strong plasmonic properties. No signs of aggregation were observed in the colloidal state, as inferred from UV-vis absorption, dynamic light scattering (DLS), and TEM studies. This proves that OAm is strongly and uniformly binding on the surface of CuNPs, thereby providing
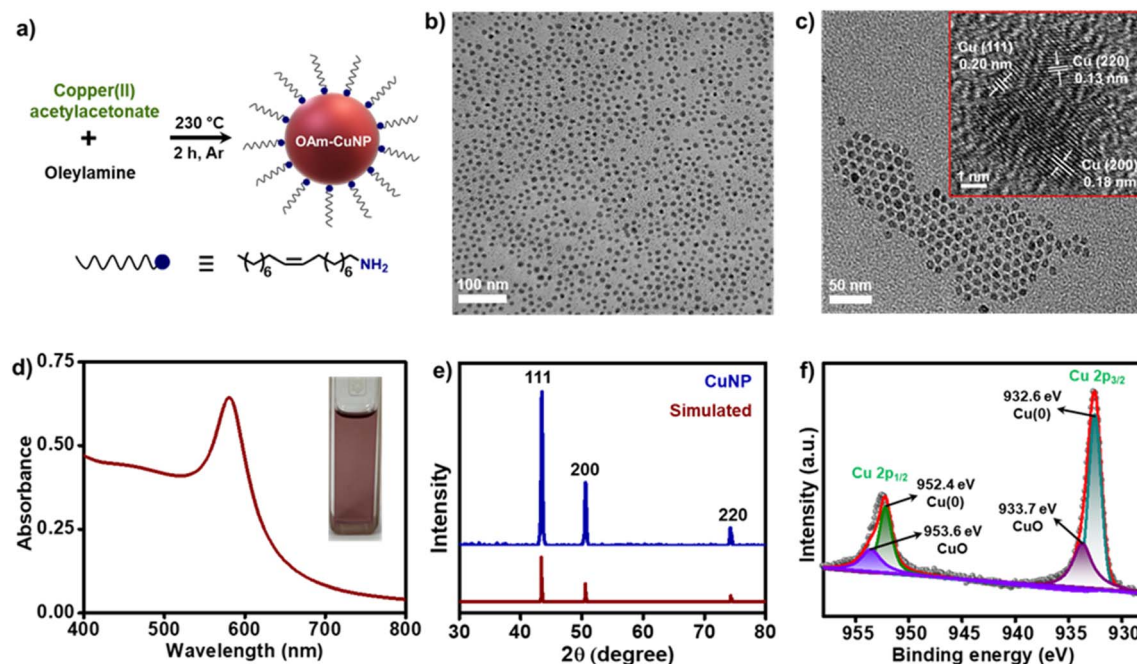
Fig. 1 Synthesis and characterization of OAm-CuNPs. (a) Schematic representation of the high-temperature protocol adopted for the synthesis of CuNPs in toluene from Cu(II) acetylacetonate. OAm acts as the reducing agent as well as the capping ligand. (b) and (c) are representative TEM images of OAm-CuNPs at two different magnifications, revealing the formation of highly monodisperse and spherical-shaped OAm-CuNPs with an average diameter of 9.0 ± 1.1 nm. The inset of (c) is the HRTEM image of a single CuNP, showing the presence of all the major lattice planes. (d) A typical UV-vis absorption spectrum of as-synthesized OAm-CuNPs in toluene, along with its optical photograph in the inset. (e) PXRD data showing the close similarity between simulated (COD ID #9012954) and experimentally obtained diffraction peaks of CuNPs. No peaks corresponding to oxidized Cu were observed in the PXRD spectrum of CuNPs. (f) The XPS spectrum of Cu shows four peaks in the Cu 2p region centered around 932 eV and 952 eV corresponding to Cu $2p_{3/2}$ and $2p_{1/2}$ core-energy levels, respectively in CuNPs.

the much-required colloidal stability in toluene (Fig. 1b, c and S2†). The powder X-ray diffraction (PXRD) pattern matches well with the simulated spectrum of Cu(0) confirming the formation of oxide-free CuNPs (Fig. 1e). Additionally, the presence of (111), (200), and (220) crystal planes corroborates well with the HRTEM studies. It is important to note here that no peaks corresponding to oxidized Cu were observed in the PXRD of CuNPs. Further, the X-ray photoelectron spectroscopy (XPS) survey spectrum confirms the presence of all major elements in CuNPs, such as Cu, C, O and N (Fig. S3†). The high-resolution XPS spectrum of Cu shows four peaks in the Cu 2p region centered around 932 eV and 952 eV corresponding to Cu $2p_{3/2}$ and $2p_{1/2}$ core-energy levels, respectively (Fig. 1f). The peaks at 932.6 eV and 952.4 eV were attributed to Cu $2p_{3/2}$ and Cu $2p_{1/2}$ of Cu(0), and the peaks at 933.7 eV and 953.6 eV were attributed to Cu $2p_{3/2}$ and Cu $2p_{1/2}$ of CuO. All the peak positions were consistent with previous reports on CuNPs.[41] It must be noted that the Cu $2p_{3/2}$ peak of CuO is reported to appear at 933.7 eV, with a very strong satellite peak at 943.6 eV.[42] However, no sign of a satellite peak was observed around 943.6 eV in our study (Fig. 1f), confirming the negligible contamination of CuO in the as-synthesized CuNPs[41,42] (slight oxidation of CuNPs could occur during the sample preparation and measurement of XPS data). Likewise, the peaks corresponding to Cu(I) are reported to overlap with Cu(0) peaks. However, the presence of Cu(I) species can be overruled in the present study, since no diffraction peaks corresponding to the oxides of Cu were observed in PXRD

studies. All the spectroscopic and microscopic characterization studies confirm the successful formation of highly mono-dispersed CuNPs, with most of the Cu in the metallic zero-oxidation state.

Ligand exchange and dispersion of CuNPs in an aqueous medium

Surface ligands are well-known to act as 'gatekeepers' in regulating the interaction of NPs with their surroundings.[43,44] As a result, the 'ligand of choice' approach has emerged as a universal strategy to control the optoelectronic properties of nanomaterials.[43,44] Moreover, it is essential to develop protocols to enhance the colloidal stability of CuNPs in an aqueous medium to expand their scope of applications. However, such surface functionalization of CuNPs with a 'ligand of choice' is scarcely reported,[33,45] which requires immediate attention. Accordingly, a place exchange protocol was developed to replace the parent OAm ligand on as-synthesized CuNPs with ligands of both polarities, namely negatively charged 11-mercaptoundecanoate (MUA, [−]) and positively charged N,N,N-trimethyl(11-mercaptoundecyl)ammonium chloride (TMA, [+]). This led to the formation of homogenously charged CuNPs in water: [+] and [−] CuNPs (Fig. 2a). Zeta potential (ζ) studies confirm the successful functionalization of [+] and [−] thiolate ligands on the surface of CuNPs (Fig. 2b ζ = +30.3 ± 5.7 mV and −35.0 ± 3.6 mV for [+] and [−] CuNPs, respectively). As per the 'hard and soft acids and bases (HSAB)' principle, it can be concluded that
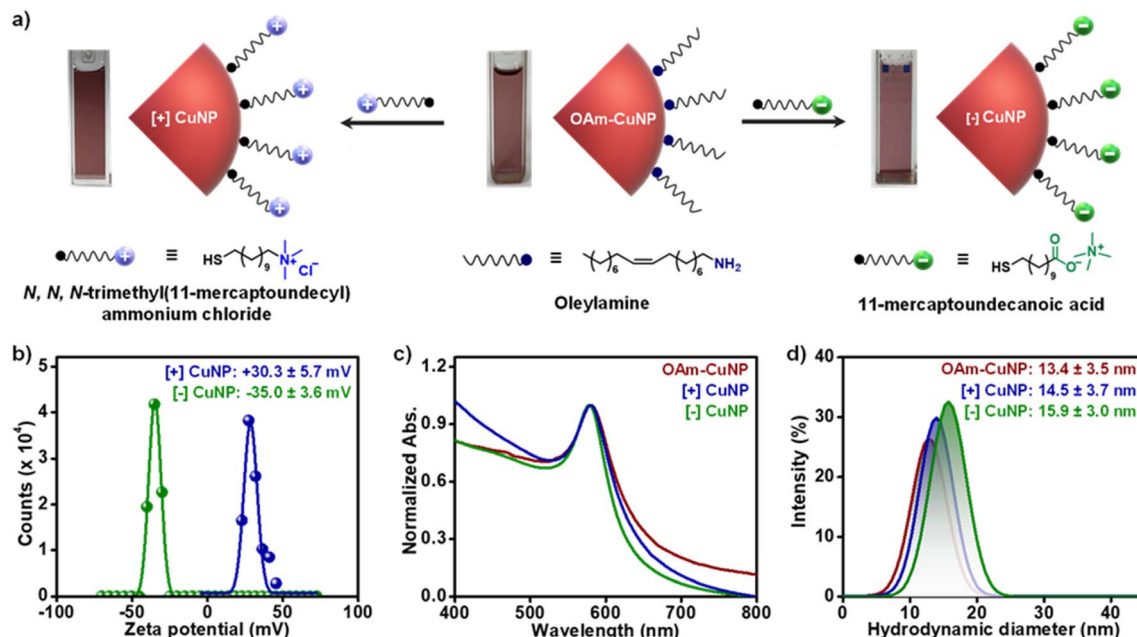
Fig. 2 Ligand exchange and dispersion of CuNPs in water. (a) Schematic representation of ligand exchange reactions, leading to the replacement of parent OAm ligands with [+] and [−] ligands. This resulted in the formation of homogenously charged CuNPs in water: [+] and [−] CuNPs. (b) Zeta potential plots of homogeneously charged CuNPs in water, proving the successful surface functionalisation of CuNPs with [+] TMA and [−] MUA ligands. (c) Normalized absorption spectra, and (d) DLS data of OAm-CuNPs in toluene, and [+] and [−] CuNPs in water. A negligible change in the LSPR band and hydrodynamic diameter after the ligand exchange reaction confirms the retention of optical properties and structural integrity of CuNPs in water.
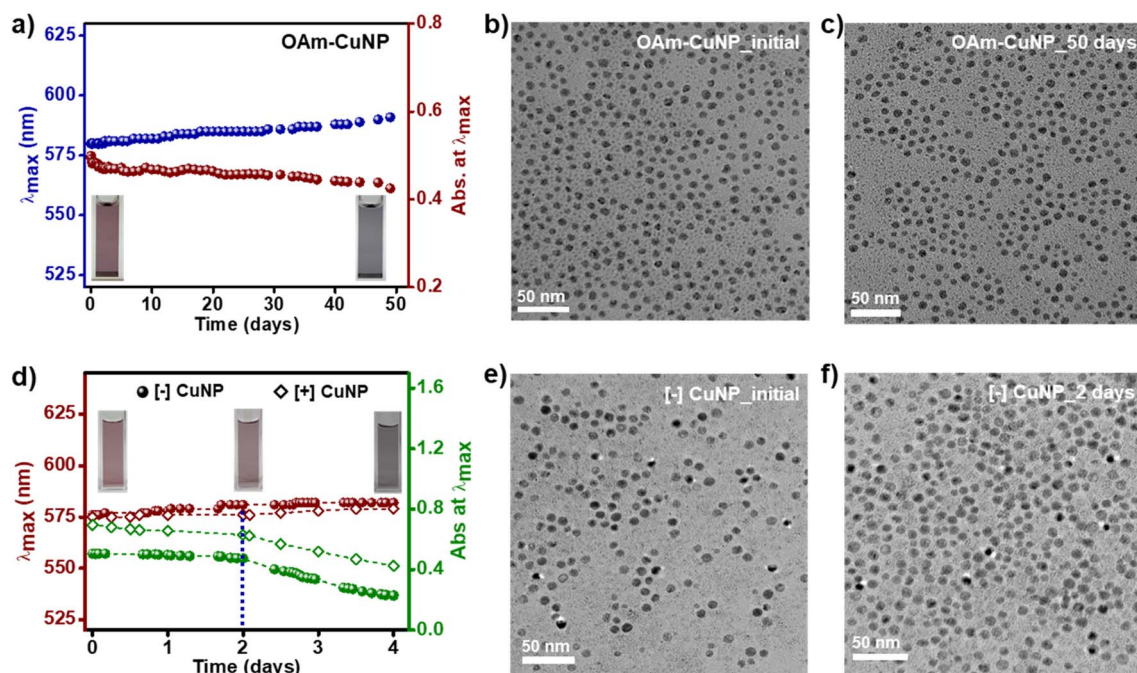

Fig. 3 Colloidal stability studies of OAm, [−], and [+] CuNPs. Time-dependent monitoring of UV-vis absorption of (a) OAm-CuNPs in toluene, (d) [−] and [+] CuNPs in water. Representative large-area TEM images of the corresponding CuNPs taken (b), (e) immediately after the synthesis and (c), (f) after a few days, as mentioned in the image. Negligible changes in the time-dependent absorption and TEM studies confirm the excellent colloidal stability of OAm-CuNPs in toluene for at least 50 days under ambient conditions. On the other hand, [−] CuNPs and [+] CuNPs could only retain their stability in aqueous medium for ~2 days under inert conditions. This lower stability could be attributed to the faster oxidation of CuNPs in water, compared to toluene.

the superior binding affinity of thiol over amine towards Cu metal was the driving force for the replacement of OAm ligands from the surface of CuNPs with TMA and MUA ligands. The presence of permanently charged quaternary ammonium and ionizable carboxylate groups of thiolate ligands impart the much-required dispersion of [+] and [−] CuNPs in aqueous medium, respectively. The characteristic LSPR band, and the color of the colloidal dispersion, were preserved after the ligand exchange reaction, confirming the retention of optical and structural integrity of CuNPs in water (Fig. 2c). A negligible change in the hydrodynamic diameter overrules the possibility of aggregation of [+] and [−] CuNPs in water, which corroborates well with the UV-vis absorption and TEM studies (Fig. 2c and d).

Colloidal stability studies of CuNPs in organic and aqueous media

Achieving the long-term stability of CuNPs, still, remains a challenging task to be resolved. Most of the previous studies either don't comment on the stability or have reported the short-term stability of CuNPs. In the present work, colloidal solutions of OAm-CuNPs, [+] CuNPs, and [−] CuNPs were prepared in respective solvents in 1 mL closed cuvette, and their stabilities were monitored using time-dependent absorption and TEM studies. It must be noted that CuNP solutions were

kept at room temperature (25 °C) during the stability studies. OAm-CuNPs retained their colloidal stability in toluene for at least 50 days under ambient conditions, with a marginal change in the λ_{LSPR} ($\Delta\lambda_{LSPR}$ ~8 nm) and shape uniformity (Fig. 3a–c, S4 and S5†). Further, [+] CuNPs and [−] CuNPs retained their stability in aqueous medium for ~2 days under inert conditions (Fig. 3d–f, S6 and S7†) and for ~6 h under ambient conditions (Fig. S8 and S9†). It must be noted that 60% absorbance of [+] and [−] CuNPs was retained in their SPR even up to ~4 days. The lower stability of CuNPs in aqueous medium can be attributed to the faster oxidation of CuNPs in water compared to toluene. This is clear from a gradual color change observed from red to black within ~4 days (Fig. S6 and S7†).[46] Even though the stability of [+] CuNPs and [−] CuNPs was comparatively lower than that of OAm-CuNPs, the obtained stability of ~2 days is sufficient for several applications including sensing and catalysis in an aqueous medium. On the other hand, it can be concluded that OAm-CuNPs showed excellent stability in toluene for at least 50 days, which proves their suitability for most of the plasmon-powered applications.

Thermoplasmonic properties of CuNPs

The long-term stability of OAm-CuNPs motivated us to study their thermoplasmonic properties and ability to raise the temperature of the surroundings *via* the plasmonic-heat
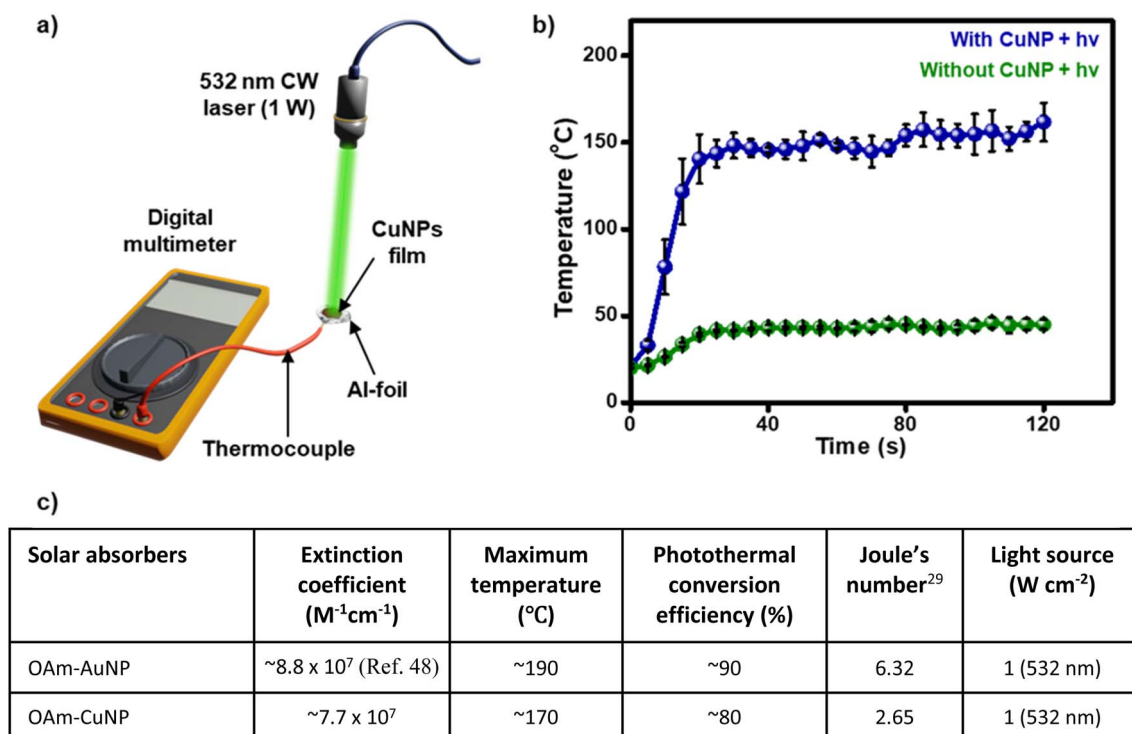

Solar absorbers	Extinction coefficient (M^{-1}cm^{-1})	Maximum temperature (°C)	Photothermal conversion efficiency (%)	Joule's number[29]	Light source (W cm^{-2})
OAm-AuNP	~8.8 x 10^7 (Ref. 48)	~190	~90	6.32	1 (532 nm)
OAm-CuNP	~7.7 x 10^7	~170	~80	2.65	1 (532 nm)

Fig. 4 Thermoplasmonic properties of OAm–CuNPs. (a) Schematics showing the experimental setup used for measuring the temperature rise caused by the plasmonic-heat generated from the CuNP film, under illumination with a 1 W 532 nm CW diode laser (the light intensity falling on the CuNP was measured to be 1 W cm^{-2}). (b) A plot showing the temperature rise measured in the presence (blue) and absence (green) of the CuNP film, under irradiation with a 1 W 532 nm CW diode laser. A sharp temperature rise was observed immediately after the laser illumination of the CuNP film, which got saturated at ~170 °C ($\Delta T \sim 150$ °C) within 30 s of illumination. Corresponding videos for the data collected in (b) are provided as Movie S1.† (c) A table comparing the plasmonic and photothermal properties of OAm–CuNPs with OAm–AuNPs, under similar experimental conditions (Fig. S10, S15 and S16†).

dissipated under light illumination. For this, a thin film of OAm-CuNPs was deposited on an aluminium film and placed on a thermocouple (Fig. 4a). An excitation source of 1 W 532 nm CW diode laser was used, as the central wavelength was close to the λ_{LSPR} band of OAm-CuNPs (the light intensity falling on the CuNP was measured to be 1 W cm^{-2}). A sharp temperature rise was observed immediately after the laser illumination, which got saturated at ~170 °C ($\Delta T \sim 150$ °C) within 30 s of illumination (rate of temperature rise was estimated to be ~5 °C s^{-1}) (Fig. 4b and Movie S1 in the ESI†). The control experiment in the absence of OAm-CuNPs showed a marginal increase in the temperature to ~45 °C ($\Delta T \sim 25$ °C) even after 5 min of illumination, which can be attributed to the thermal effect of light illumination (Fig. 4b and Movie S1 in the ESI†). Further, the photothermal conversion efficiency (η_{PT}) of OAm-CuNPs was estimated to be ~80% using a standard protocol, as described in the ESI (Fig. S10†). Photostability studies show that CuNPs retained their plasmonic properties even after prolonged illumination (Fig. S11†). Further, CuNPs were thermally stable up to 100 °C in toluene and 200 °C in oleylamine solution (Fig. S12 and S13†). At this point, it is important to estimate and compare various optical parameters of CuNPs with the benchmark AuNPs, to verify the prospects of CuNPs as an alternate plasmonic heater. For this, OAm-capped AuNPs with similar sizes were synthesized (Fig. S14†).[47] The concentrations of OAm-CuNPs and OAm-AuNPs[48] were kept constant, enabling a fair comparison between their optical properties. As clear from Fig. 4c, OAm-CuNPs possess excellent optical parameters, especially with respect to the molar extinction coefficient, rate of temperature rise, and efficiency of light-to-heat energy conversion. Even though the conventional plasmonic AuNPs have a larger rise in local temperature, the ΔT of ~150 °C achieved with plasmonic CuNPs was 'hot' enough to perform high-temperature chemical and physical transformations as described in the next section. More importantly, Fig. 4c provides some of the key fundamental plasmonic and photothermal parameters such as molar extinction coefficient, photothermal conversion efficiency, and the temperature rise due to plasmonic-heat, that are currently missing in the literature on CuNPs. Thus, CuNPs satisfy all the fundamental optical properties required to emerge as an affordable alternative to conventional plasmonic NPs for various visible-light-driven processes.

Solar-vapor generation with plasmonic CuNP heaters

The strong photothermal properties of OAm-CuNPs (η_{PT} ~80% and $\Delta T \sim 150$ °C) motivated us to use the plasmonic-heat generated from CuNPs for high-temperature photothermal applications. Also, a strong overlap between the solar spectrum and the extinction spectrum of CuNPs justifies the suitability of
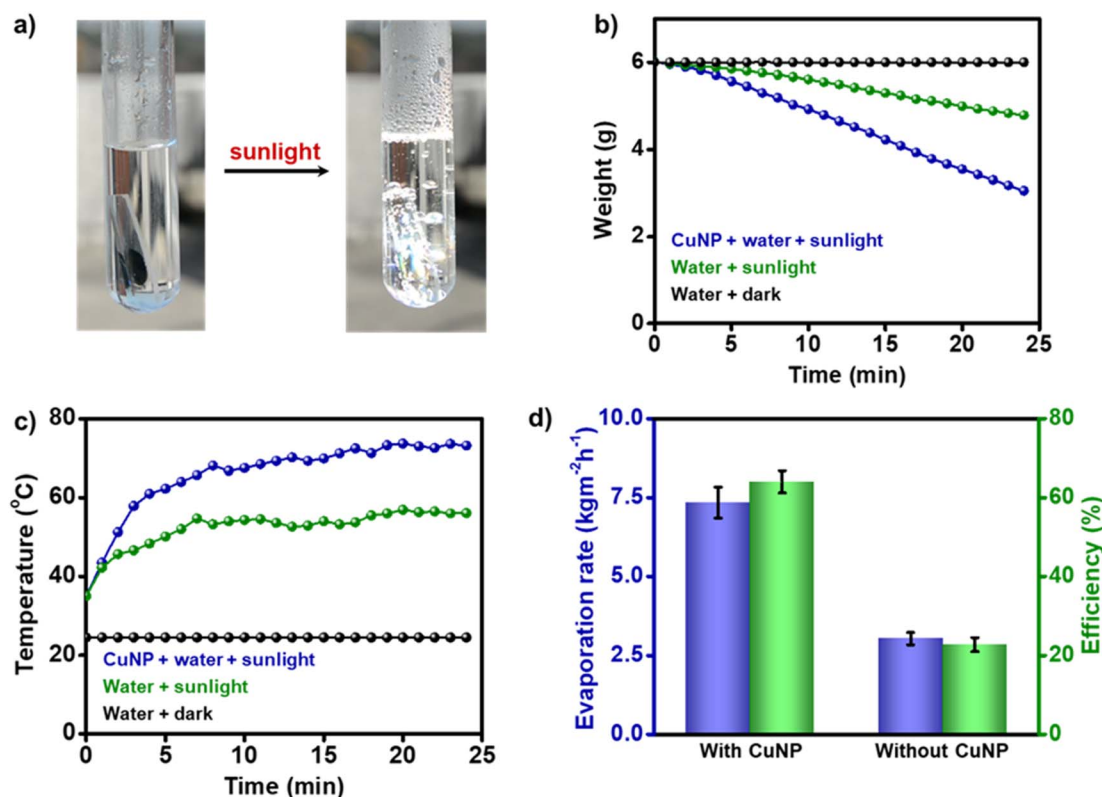

Fig. 5 Solar-vapor generation with plasmonic CuNP heaters. (a) Optical photographs for the boiling of water triggered by the plasmonic-heat generated from CuNPs, illuminated under focused sunlight. (b) Weight loss and (c) temperature change with respect to time, for different sets of experiments (water + dark represents the experiment done in the dark inside the laboratory at room temperature ~25 °C). (d) A graph showing the efficiency and rate of solar-vapor evaporation in the presence and absence of plasmonic CuNPs. The error bars correspond to data collected from three independent samples of CuNPs.

plasmonic CuNP heaters for sunlight-triggered chemical and physical transformations. As a proof of concept, the chemical effectiveness of the plasmonic-heat dissipated by CuNPs was tested in solar-vapor generation, which is one of the standard experiments performed in thermoplasmonics.[7,49] Along with being an effective approach for water-desalination and steam-generation processes, the solar-vapor generation experiment can be used as a model study for comparing the efficiency of plasmonic heaters. Focused solar illumination of a CuNP-coated glass film suspended in water resulted in the instantaneous boiling of water (the sunlight was focused using a 19.5 cm × 28.5 cm Fresnel lens). Steam generation was clearly observed along with vigorous boiling and condensation of water on the sides of the test tube (Fig. 5a, S17 and Movie S2 in the ESI†). Approximately 3 g of water was evaporated within ∼25 minutes of solar illumination, and the temperature of the bulk water increased to ∼75 °C ($\Delta T \sim 40$ °C) (Fig. 5b and c). Control experiments confirmed the active role of sunlight-triggered plasmonic-heat generated from CuNPs in the solar-vapor generation (Fig. S18†). The rate and efficiency of evaporation were estimated to be ~ 7.7 kg m^{-2} h^{-1} and $\sim 66\%$, respectively (Fig. 5d and S19, see the ESI† for calculation). There have been a couple of previous studies on solar-vapor generation with Cu-based materials; however, they were either with CuNPs embedded in a cellulose support or with Cu in micro-dimensions (Table S1†). The solar vapor generation parameters for CuNPs reported here are some of the best among the Cu-based nanostructures studied so far and comparable with those of the benchmark AuNPs (Table S1†), with the added advantage of cost-effectiveness.

Thermochromism with plasmonic CuNP heaters

Thermochromic molecules are well-known to show temperature-dependent color changes, corresponding to
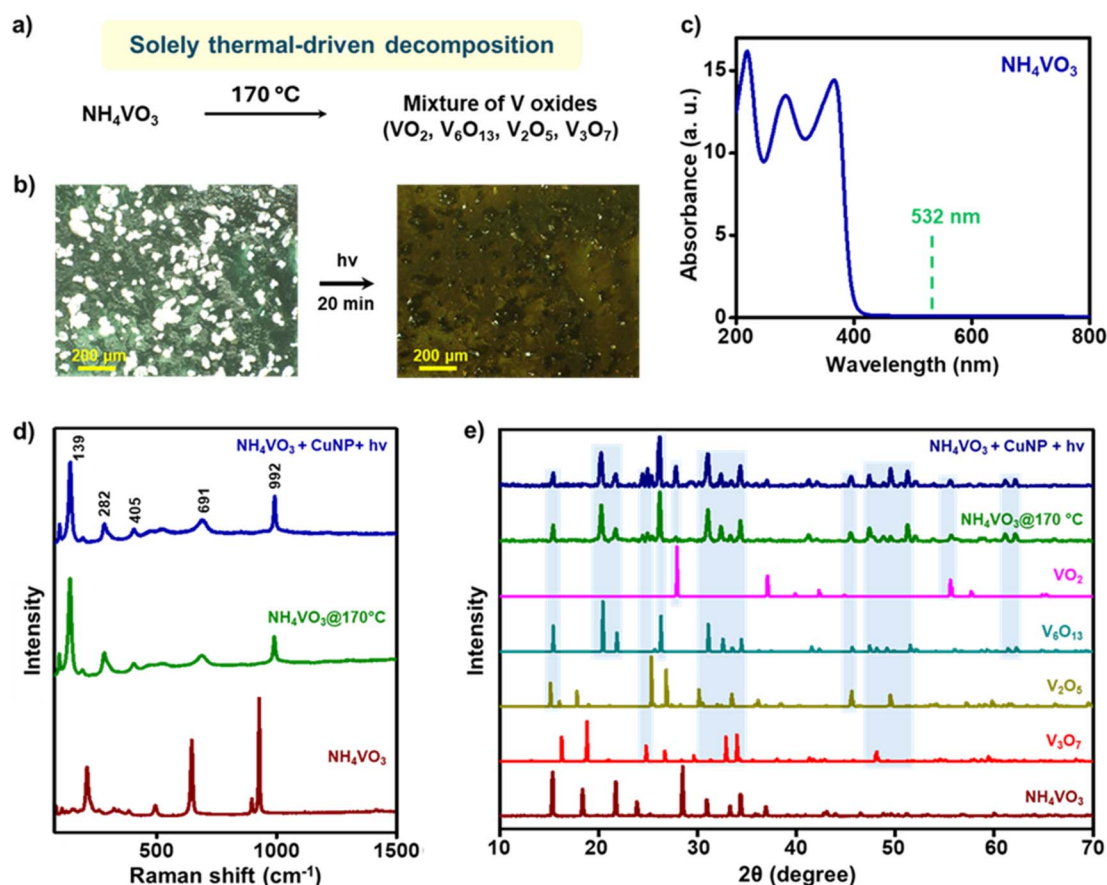
Fig. 6 High-temperature crystal-to-crystal phase transformation with plasmonic CuNP heaters. (a) Scheme for the thermal decomposition reaction of NH_4VO_3 into its mixture of oxides. (b) Left: optical microscopic image of a magnified area of the CuNP film coated on a glass slide (green area), onto which NH_4VO_3 was uniformly distributed (white powder). Right: a clear colour change from white to black was observed, within ∼20 min of irradiation of the CuNP film with a 1 W 532 nm CW diode laser (light intensity was estimated to be 1 W cm^{-2}). The plasmonic-heat generated from CuNPs was sufficient to cause an irreversible thermochromic phase change in NH_4VO_3. (c) Solid-state UV-visible absorption spectrum of NH_4VO_3 shows negligible absorbance around 532 nm. The solid-state absorption was measured in the reflectance mode. Diffuse reflectance data was converted to absorbance using the Kubelka–Munk transformation. (d) Raman and (e) PXRD studies confirm the similar structural identity of the black vanadium oxide crystals formed from thermoplasmonically (blue spectrum) and thermally treated NH_4VO_3 (olive green spectrum). PXRD studies confirm that a mixture of oxides of vanadium was formed from both thermoplasmonically and thermally treated NH_4VO_3. The reference simulated PXRD patterns for all the expected products (oxides of vanadium) are included for comparison. The color bars show the overlap of major diffraction peaks in thermoplasmonically and thermally treated NH_4VO_3 samples, with the reference peaks.

specific crystal-to-crystal phase transformations.[50] Recently, irreversible-thermochromic molecules have been used as a pseudo-thermometer for measuring the minimum temperature rise caused by the plasmonic-heat dissipated from AuNPs.[20] Here, we have tested the potential of the plasmonic-heat generated from OAm-CuNPs in causing a phase transition in an irreversible-thermochromism molecule named, ammonium metavanadate (NH_4VO_3). NH_4VO_3 is reported to show a thermochromic change from white → yellow → black colour at 150 °C and 170 °C, respectively, corresponding to its thermal decomposition to a mixture of oxides of vanadium.[50] Further, the irreversible-thermochromism in NH_4VO_3 is a solely thermal-driven reaction (Fig. 6a). In the present study, the white crystals of NH_4VO_3 were adsorbed onto the OAm-CuNP coated glass film, followed by irradiation with a 1 W 532 nm CW diode laser (the light intensity falling on the CuNP film was measured to be 1 W cm^{-2}). A clear color change from white → yellow → black was observed within ~20 min of irradiation, confirming the irreversible-thermochromic transformation (Fig. 6b, S20a, and Movie S3†). The control experiment performed in the absence of CuNPs failed to show any thermochromic transformation (Fig. S20b and S21†). In another control experiment, the white crystals of NH_4VO_3 were thermally treated at ~170 °C, which led to the expected color change from white to black. NH_4VO_3 has a negligible absorption at the illumination wavelength of 532 nm, which rules out the possibility of any nonthermally activated chromism effect, such as photochemical transformation (Fig. 6c). The Raman and powder X-ray diffraction (PXRD) patterns for thermoplasmonically and thermally treated NH_4VO_3 matched very well with each other (Fig. 6d and e). The PXRD studies confirm the formation of a mixture of oxides of vanadium (tetragonal-VO_2, monoclinic-V_6O_{13}, orthorhombic-V_2O_5, and monoclinic-V_3O_7) in both thermoplasmonically and thermally treated NH_4VO_3. All these experiments conclusively prove that the plasmonic-heat generated from OAm-CuNPs can raise the surrounding temperature to at least 170 °C, which was sufficient to cause a crystal-to-crystal phase transition in NH_4VO_3. It must be mentioned that the temperature rise reported using the thermochromism study is the lower limit, and the actual surface temperature on CuNPs might be higher. A separate study could be performed in the future to determine the actual surface temperature of plasmonic CuNPs under illumination with the help of standard nanothermometry techniques.[51] Despite that, the present study unambiguously confirms that the temperature was raised to at least ~170 °C by the plasmonic-heat generated from CuNPs, which was 'hot' enough to perform useful high-temperature chemical and physical transformations.

Conclusions

A high-temperature in situ reduction method has been adopted for the synthesis of highly monodisperse and spherical-shaped CuNPs, with an average core diameter of ~9.0 ± 1.1 nm. The characteristic λ_{LSPR} band centered at ~580 nm (wine-red color) and corresponding crystallography studies confirm that most of the Cu present in CuNPs is in the metallic zero-oxidation state.

The light absorbing power of CuNPs was estimated to be ~7.7 × 10^7 M^{-1} cm^{-1} at 580 nm, which is comparable to that of the benchmark plasmonic AuNPs. OAm-CuNPs showed excellent stability in toluene for at least 50 days under ambient conditions, without any noticeable change in their optical properties. Using a ligand exchange protocol, the surface of CuNPs was decorated with charged thiolate ligands to yield a stable dispersion of CuNPs in water (for ~2 days and ~6 h under inert and ambient conditions, respectively). This led to the formation of stable and homogeneously charged [+] and [−] CuNPs. Photothermal studies prove that the plasmonic-heat generated from CuNPs can raise the surrounding temperature to ~170 °C, within ~30 s of illumination with a 1 W 532 nm CW diode laser (light intensity was estimated to be 1 W cm^{-2}). The strong photothermal properties of OAm-CuNPs (η_{PT} ~80% and ΔT ~ 150 °C) motivated the use of CuNPs as plasmonic heaters for high-temperature photothermal applications, such as solar-vapor generation and thermochromism. The thermo-plasmonic properties of CuNPs were comparable to those of some of the best conventional plasmonic materials reported, which makes CuNPs an affordable plasmonic heater for future photothermal applications. A series of studies could emerge soon by using CuNPs in other plasmon-mediated studies such as plasmonic photocatalysis and nearfield enhancement studies. In summary, our work reports key visible-light driven plasmonic and photothermal properties of CuNPs, which is expected to open a whole new dimension in plasmon-powered research with earth-abundant materials.

Data availability

The article and the ESI† contain data supporting the findings of the study. The corresponding author will provide appropriate source data upon reasonable request.

Author contributions

S. T. and R. K. K. prepared and characterized CuNPs with the help of A. D. S. T. performed the stability studies. R. K. K. performed the photothermal conversion efficiency measurements with the help of S. T. A. D. performed the XPS analysis. All the thermoplasmonic studies were performed by S. T., R. K. K. and A. D. All authors contributed to the discussion, writing, and provided feedback on the manuscript. P. P. P. conceived the project and coordinated the research.

Conflicts of interest

There are no conflicts to declare.

Acknowledgements

Notes and references

1 S. Link and M. A. El-Sayed, *J. Phys. Chem. B*, 1999, **103**, 8410–8426.

2 J. H. Hodak, I. Martini and G. V. Hartland, *J. Phys. Chem. B*, 1998, **102**, 6958–6967.

3 M. L. Brongersma, N. J. Halas and P. Nordlander, *Nat. Nanotechnol.*, 2015, **10**, 25–34.

4 U. Aslam, V. G. Rao, S. Chavez and S. Linic, *Nat. Catal.*, 2018, **1**, 656–665.

5 P. K. Jain, *J. Phys. Chem. C*, 2019, **123**, 24347–24351.

6 V. Jain, R. K. Kashyap and P. P. Pillai, *Adv. Opt. Mater.*, 2022, **10**, 2200463.

7 O. Neumann, A. S. Urban, J. Day, S. Lal, P. Nordlander and N. J. Halas, *ACS Nano*, 2013, **7**, 42–49.

8 C. Wang, O. Ranasingha, S. Natesakhawat, P. R. Ohodnicki, M. Andio, J. P. Lewis and C. Matranga, *Nanoscale*, 2013, **5**, 6968–6974.

9 C. Fasciani, C. J. B. Alejo, M. Grenier, J. C. Netto-Ferreira and J. C. Scaiano, *Org. Lett.*, 2011, **13**, 204–207.

10 L. R. Hirsch, R. J. Stafford, J. A. Bankson, S. R. Sershen, B. Rivera, R. E. Price, J. D. Hazle, N. J. Halas and J. L. West, *Proc. Natl. Acad. Sci. U.S.A.*, 2003, **100**, 13549–13554.

11 X. Huang, I. H. El-Sayed, W. Qian and M. A. El-Sayed, *J. Am. Chem. Soc.*, 2006, **128**, 2115–2120.

12 M. Dhiman, A. Maity, A. Das, R. Belgamwar, B. Chalke, Y. Lee, K. Sim, J.-M. Nam and V. Polshettiwar, *Chem. Sci.*, 2019, **10**, 6594–6603.

13 J. C. Ndukaife, V. M. Shalaev and A. Boltasseva, *Science*, 2016, **351**, 334–335.

14 B. Klemmed, L. V. Besteiro, A. Benad, M. Georgi, Z. Wang, A. Govorov and A. Eychmüller, *Angew. Chem., Int. Ed.*, 2019, **59**, 1696–1702.

15 J. Gargiulo, M. Herran, I. L. Violi, A. Sousa-Castillo, L. P. Martinez, S. Ezendam, M. Barella, H. Giesler, R. Grzeschik, S. Schlücker, S. A. Maier, F. D. Stefani and E. Cortés, *Nat. Commun.*, 2023, **14**, 1–11.

16 A. S. Urban, M. Fedoruk, M. R. Horton, J. O. Rädler, F. D. Stefani and J. Feldmann, *Nano Lett.*, 2009, **9**, 2903–2908.

17 J. Qiu, Y.-C. Wu, Y.-C. Wang, M. H. Engelhard, L. McElwee-White and W. D. Wei, *J. Am. Chem. Soc.*, 2013, **135**, 38–41.

18 A. O. Govorov and H. H. Richardson, *Nano Today*, 2007, **2**, 30–38.

19 R. K. Kashyap, S. Tyagi and P. P. Pillai, *Chem. Commun.*, 2023, **59**, 13293–13296.

20 R. K. Kashyap, I. Dwivedi, S. Roy, S. Roy, A. Rao, C. Subramaniam and P. P. Pillai, *Chem. Mater.*, 2022, **34**, 7369–7378.

21 R. K. Kashyap, M. J. Parammal and P. P. Pillai, *ChemNanoMat*, 2022, **8**, e202200252.

22 R. K. Kashyap and P. P. Pillai, *Nano Lett.*, 2024, **24**, 5585–5592.

23 G. V. Naik, V. M. Shalaev and A. Boltasseva, *Adv. Mater.*, 2013, **25**, 3264–3294.

24 M. B. Gawande, A. Goswami, F.-X. Felpin, T. Asefa, X. Huang, R. Silva, X. Zou, R. Zboril and R. S. Varma, *Chem. Rev.*, 2016, **116**, 3722–3811.

25 M. W. Knight, N. S. King, L. Liu, H. O. Everitt, P. Nordlander and N. J. Halas, *ACS Nano*, 2014, **8**, 834–840.

26 G. Zhou, M. Hou, Y. Ren, Z. Jiang and N.-C. Lai, *J. Energy Storage*, 2023, **72**, 108458.

27 M. Dasog, *Chem. Mater.*, 2022, **34**, 4249–4258.

28 T. M. Mattox, X. Ye, K. Manthiram, P. J. Schuck, A. P. Alivisatos and J. J. Urban, *Adv. Mater.*, 2015, **27**, 5830–5837.

29 A. Lalisse, G. Tessier, J. Plain and G. Baffou, *J. Phys. Chem. C*, 2015, **119**, 25518–25528.

30 N. A. Dhas, C. P. Raj and A. Gedanken, *Chem. Mater.*, 1998, **10**, 1446–1452.

31 M. A. B. Aissa, B. Tremblay, A. Andrieux-Ledier, E. Maisonhaute, N. Raouafi and A. Courty, *Nanoscale*, 2015, **7**, 3189–3195.

32 F. M. Alcorn, R. M. van der Veen and P. K. Jain, *Nano Lett.*, 2023, **23**, 6520–6527.

33 Y. Wei, S. Chen, B. Kowalczyk, S. Huda, T. P. Gray and B. A. Grzybowski, *J. Phys. Chem. C*, 2010, **114**, 15612–15616.

34 Y. Lin, Z. Chen, L. Fang, M. Meng, Z. Liu, Y. Di, W. Cai, S. Huang and Z. Gan, *Nanotechnology*, 2019, **30**, 015402.

35 A. Marimuthu, J. Zhang and S. Linic, *Science*, 2013, **339**, 1590–1593.

36 I. S Pieta, R. G. Kadam, P. Pieta, D. Mrdenovic, R. Nowakowski, A. Bakandritsos, O. Tomanec, M. Petr, M. Otyepka, R. Kostecki, M. A. M. Khan, R. Zbořil and M. B. Gawande, *Adv. Mater. Interfaces*, 2021, **8**, 2001822.

37 A. D. Kute, R. P. Gaikwad, I. R. Warkad and M. B. Gawande, *Green Chem.*, 2022, **24**, 3502–3573.

38 H. B. Kale, A. D. Kute, R. P. Gaikwad, P. Fornasiero, R. Zbořil and M. B. Gawande, *Coord. Chem. Rev.*, 2024, **502**, 215602.

39 P. Fan, H. Wu, M. Zhong, H. Zhang, B. Bai and G. Jin, *Nanoscale*, 2016, **8**, 14617.

40 Y. Wang, Q. Zhang, Y. Wang, L. V. Besteiro, Y. Liu, H. Tan, Z. M. Wang, A. O. Govorov, J. Z. Zhang, J. K. Cooper, J. Zhao, G. Chen, M. Chaker and D. Ma, *Chem. Mater.*, 2021, **33**, 695–705.

41 Z.-J. Zuo, J. Li, P.-D. Han and W. Huang, *J. Phys. Chem. C*, 2014, **118**, 20332–20345.

42 T. Subashchandrabose, M. Madasu, C.-F. Hsia, D.-Y. Liu and M. H. Huang, *Chem.–Asian J.*, 2017, **12**, 2318–2322.

43 V. Jain, S. Roy, P. Roy and P. P. Pillai, *Chem. Mater.*, 2022, **34**, 7579–7597.

44 J. Kuno, T. Kawai and T. Nakashima, *Nanoscale*, 2017, **9**, 11590–11595.

45 M. Shi, H. S. Kwon, Z. Peng, A. Elder and H. Yang, *ACS Nano*, 2012, **6**, 2157–2164.

46 R. L. Calabro, F. J. Burpo, S. F. Bartolucci and J. A. Maurer, *J. Phys. Chem. C*, 2023, **127**, 15307–15315.

47 S. Liu, G. Chen, P. N. Prasad and M. T. Swihart, *Chem. Mater.*, 2011, **23**, 4098–4101.

48 X. Liu, M. Atwater, J. Wang and Q. Huo, *Colloids Surf., B*, 2007, **58**, 3–7.

49 M. J. Margeson and M. Dasog, *Environ. Sci.: Water Res. Technol.*, 2020, **6**, 3169–3177.

50 A. A. Akande, E. C. Linganiso, B. P. Dhonge, K. E. Rammutla, A. Machatine, L. Prinsloo, H. Kunert and B. W. Mwakikunga, *Mater. Chem. Phys.*, 2015, **151**, 206–214.

51 G. Baffou, *Thermoplasmonics: Heating Metal Nanoparticles Using Light*, Cambridge University Press, 2017.